ICARUS 101, 1–17 (1993)

Equatorial Superrotation in a Slowly Rotating GCM: Implications for Titan and Venus

ANTHONY D. DEL GENIO

NASA Goddard Institute for Space Studies, New York, New York 10025

AND

WEI ZHOU AND TIMOTHY P. EICHLER

ST Systems Corporation, Institute for Space Studies, New York, New York 10025

Received July 17, 1992; revised October 5, 1992

The maintenance of strong superrotating zonal winds in the equatorial Venus atmosphere and the possibility of a similar regime on Titan are examined with a modified version of an efficient terrestrial general circulation model (GCM). The model is simplified by removal of the hydrologic cycle, the diurnal cycle, and all seasonal and geographic variations. We describe a suite of equilibrium simulations in which rotation rate, radiative heating profile, surface drag, and stratospheric drag are varied. The key to superrotation in these experiments is the presence of an upper troposphere cloud which intercepts much of the incoming solar flux and produces a statically stable radiative equilibrium state in the lower and middle troposphere. The radiative heating profile limits the depth of boundary layer convection and detaches the upper level flow from the surface. At Titan's presumed rotation period, the cloud-covered GCM produces equatorial winds in excess of 50/100 m sec^{-1} with/without stratospheric drag. Superrotation extends throughout most of the atmosphere. Hadley cell interaction with quasi-barotropic eddies which transport momentum equatorward is responsible for the excess angular momentum, confirming certain aspects of proposals by Gierasch (1975) and Rossow and Williams (1979) but with relatively modest Prandtl numbers. The latitudinal profile of zonal wind resembles that for uniform absolute *linear* momentum. Removal of the cloud decreases static stability, increases vertical convective mixing, and almost completely eliminates equatorial superrotation. Equatorial winds >60 m sec^{-1} also occur at Venus' rotation period, but only near the upper boundary in the absence of stratospheric drag. In the slowly rotating regime, equatorial winds increase as surface drag increases. Our calculations represent the first GCM simulation of strong superrotation without unrealistic momentum sources. The results suggest that superrotation is not inevitable on slowly rotating planets but is likely if diabatic heating produces a statically stable thermal structure.

1. INTRODUCTION

One of the most surprising aspects of planetary fluid dynamics has been the observation that Venus, the most slowly rotating planet in the Solar System (rotation period = 243 days), has strong planetwide superrotating zonal winds whose angular velocity is 50–60 times that of the solid planet. This finding was anticipated by groundbased observers and verified by a variety of spacecraft instruments (cf. Rossow *et al.* 1990 for a review of the observations).

Titan, which presumably is tidally locked to Saturn, appears to be in a similar dynamical regime (rotation period = 16 days). Midlatitude superrotation on Titan has been inferred from IR brightness temperatures (Flasar *et al.* 1981), and tentative suggestions of stratospheric low-latitude superrotation also exist (Wenkert and Garneau 1987, Sicardy *et al.* 1990), but there is no direct evidence and no information at all below Titan's tropopause.

The dynamics of both Venus and Titan are driven by latitudinally varying insolation. It is therefore easy to understand the presence of middle or high latitude superrotation on these planets as the consequence of poleward angular momentum transport by a thermally direct Hadley circulation. *Equatorial* superrotation, however, requires the presence of nonaxisymmetric eddy motions (Hide 1969, Held and Hou 1980, Rossow 1985). A number of mechanisms for producing such eddies have been proposed, including barotropic instability of the high-latitude jet produced by the Hadley cell (Gierasch 1975, Rossow and Williams 1979), solar semidiurnal thermal tides (cf. Fels and Lindzen 1974, Pechmann and Ingersoll 1984,

0019-1035/93 $5.00

Leovy 1987), transient or topographically forced planetary- or small-scale gravity waves (Leovy 1973, Hou and Farrell 1987, Gierasch 1987, Del Genio and Rossow 1990), and external torques (Gold and Soter 1971).

GCMs predict the existence of high-latitude jets when run at slow rotation, but they have been unsuccessful in generating equatorial superrotation. The only GCMs to date which have produced strong equatorial winds did so in the presence of unrealistic momentum sources, e.g., due to a nonconservative eddy diffusion parameterization (Young and Pollack 1977). Other slowly rotating GCMs have yielded weak or even subrotating zonal winds at the equator despite the presence of quasi-barotropic eddies which transport momentum equatorward as required by the Gierasch–Rossow–Williams scenario (Rossow 1983, Covey *et al.* 1986, Del Genio and Suozzo 1987). Since none of the latter group of models included a diurnal cycle, it was plausible to speculate that missing transports by thermal tides are the crucial superrotation mechanism. Williams (1988a,b) in fact achieves moderate equatorial superrotation via diurnal forcing of a moist terrestrial GCM. This is appropriate for the upper Venus atmosphere, but much stronger than that experienced by either the deep Venus atmosphere or Titan's atmosphere. Consistent with this view, Hou *et al.* (1990), using a high-resolution tidal model coupled to a zonally averaged circulation model, have demonstrated that tides act primarily within and above the cloud layer on Venus and can account for only about half of the observed superrotation.

Del Genio and Suozzo (1987) suggested that the failure of slowly rotating GCMs to superrotate was a consequence of excessive vertical mixing by parameterized convection driven by statically unstable radiative equilibrium temperature profiles. The convection mixes momentum downward where it is transferred to the solid planet by surface drag, and the adiabatic thermal structure prevents large vertical wind shears. The resulting weakly stable lapse rate inhibits the development of quasi-barotropic eddies. In slowly rotating terrestrial GCMs, the radiative state is dictated by the semitransparency of Earth's atmosphere to sunlight, which is absorbed mostly at the surface. In the Venus GCM of Rossow (1983), the radiative equilibrium state was specified to be superadiabatic in the lowest 20 km, according to prevailing opinion about the Venus thermal structure at that time. Pioneer Venus, Venera, and Vega probes have since shown, however, that the Venus atmosphere is statically stable above 5 km altitude except for isolated near-neutral layers at ~25–30 km and ~50–55 km (cf. Young *et al.* 1987). Titan radio occultation temperature profiles from the Voyager mission are also statically stable above ~3.5 km altitude (Lindal *et al.* 1983), although the possibility of methane moist convection on Titan complicates assessments of the strength of vertical mixing there.

In this paper we use the GISS GCM to examine the hypothesis that equatorial superrotation on slowly rotating planets is sensitive to the nature of the vertical radiative heating profile (and resulting static stability) and can exist in the absence of diurnally varying forcing. Section 2 describes the GISS GCM, the modifications we have made for this investigation, and the simulations that were carried out. Section 3 describes the general circulation, diabatic heating, and thermal structure produced in the experiments. In Section 4 we analyze the heat and angular momentum budgets and energy cycles to understand the factors conducive to equatorial superrotation. In Section 5 we evaluate our results in light of Gierasch's original hypothesis and discuss their implications for future planetary missions.

2. MODEL AND SIMULATION DESCRIPTIONS

The simulations were performed with the Model II version of the GISS GCM (Hansen *et al.* 1983). Model II is a gridpoint model with approximately 8° × 10° horizontal resolution and nine vertical levels with an upper boundary at 10 mbar pressure. The vertical differencing scheme uses the σ-coordinate system. Horizontal differencing uses the schemes of Arakawa (1972) on the B-grid, except that potential temperature replaces temperature as a prognostic variable. The model requires approximately 1.1 hr CPU time per simulated month on an Amdahl 5870 computer.

An important feature of the GISS GCM is that its stable numerical schemes permit the model to be run with no explicit horizontal or vertical diffusion. The Arakawa differencing techniques conserve global angular momentum to within about 0.0005% per day, or 1–10% over an entire integration of the model to equilibrium, with the numerics acting as a very weak momentum sink. This assures that any superrotation which occurs is the result of explicitly resolved and/or parameterized physical processes.

Physics parameterizations for Model II are described fully in Hansen *et al.* (1983). Important features for this application of the model include: (i) Radiative heating, computed with a semi-implicit spectral integration including all significant atmospheric gases, aerosols, and cloud particles. (ii) Dry convective adjustment, which completely mixes heat and momentum when two adjacent layers are statically unstable and produces a dry adiabatic radiative–convective thermal structure where it occurs. (iii) Surface fluxes of heat and momentum, obtained from a drag-law formulation with a specified drag coefficient; this differs from the standard version of the GCM, in which the drag coefficient varies empirically with stability based on observations of the terrestrial boundary layer. The dimensionless drag coefficient C_D is chosen to be either 4×10^{-3} or 4×10^{-4} in each run; these bracket the

values typically encountered on Earth and are fairly close to the upper and lower limits for land- and ocean-covered surfaces estimated for Titan by Allison (1992). (iv) Stratospheric drag, parameterized as a simple Rayleigh friction with a wind-dependent drag coefficient acting only in the model's uppermost level; this is a very crude representation of the effects of breaking waves, but it serves in terrestrial simulations to close off the jet stream at the tropopause as observed.

In principle, the simplest test of superrotation theories would be a direct simulation of the Venus and Titan atmospheres, with accurate specifications of atmospheric mass and composition, radiative heating, and planetary radius and surface properties for each planet. For Titan especially, these characteristics are rather poorly known. The bigger obstacle, however, is that Venus' massive atmosphere and Titan's large distance from the Sun yield radiative relaxation times of the order of 50–150 years for both planets (Pollack and Young 1975, Flasar *et al.* 1981). Stone (1974) shows that the adjustment of the circulation to equilibrium occurs on the radiative relaxation time scale if the radiative equilibrium state is statically stable, as is generally the case for both planets. Since the transient and equilibrium behaviors of the general circulation are not necessarily identical, Titan and Venus models would have to run for several hundred simulated years to provide a reliable diagnosis of superrotation mechanisms. The excessive CPU requirements of such runs would preclude sensitivity testing necessary to elucidate the factors which control superrotation.

Our approach is to run the GCM instead as a terrestrial model with several key parameters changed to mimic the important differences between Venus, Titan, and Earth. The GCM thus has a surface pressure of 1 bar, terrestrial atmospheric composition and planetary radius, and a solar constant appropriate to 1 AU. The model is initialized with an isothermal, motionless state and run to equilibrium (typically 5–10 years), as judged by the temporal evolution of the global angular momentum, energy cycle components, surface and air temperature, wind components, and diabatic heating. Diagnostics are then accumulated and averaged over an additional 5-year period. This strategy permits us to conduct six sensitivity experiments in less CPU time than would be required for a single integration to equilibrium of either Venus' or Titan's atmosphere.

To simplify the GCM, we remove the diurnal and seasonal cycles as well as topography and all geographic variations. Each of these may actually play an important role on either Venus or Titan. However, by doing so we eliminate the possibility of thermal tides or orographic gravity waves, and this enables us to evaluate the importance of the Gierasch–Rossow–Williams superrotation mechanism in isolation from all other effects. We furthermore suppress the model's hydrologic cycle in the current experiments by eliminating evaporation, condensation, and precipitation. Water vapor is thus a well-mixed gas with neither sources nor sinks and acts solely as a radiatively active constituent. The model's surface is prescribed to have the properties of a flat terrestrial desert.

TABLE I
Parameter Settings for GCM Experiments

Experiment	Rotation period (days)	Cloud τ	Surface drag coefficient	Stratospheric drag
T1	16	5	4×10^{-3}	Yes
T2	16	0	4×10^{-3}	Yes
T3	16	5	4×10^{-3}	No
T4	16	5	4×10^{-4}	Yes
V	243	5	4×10^{-3}	No
E	1	5	4×10^{-3}	Yes

The GCM's predicted clouds are replaced by a prescribed planetwide cloud layer with the optical properties of 10-μm water droplets as is normally parameterized in the terrestrial version of the GCM. The cloud is assumed for this paper to occupy three model layers between the 150- and 550-mbar levels. The optical thickness is chosen so that the cloud intercepts a substantial portion of the incoming solar flux and the resulting radiative heating produces a statically stable layer not far above the surface. We choose an optical thickness $\tau = 5$ at 0.5-μm wavelength, which for the specified cloud and surface properties yields a 44% planetary albedo, with 36% of the insolation being absorbed at the surface. Sensitivity tests with thicker clouds (up to $\tau = 120$) do not qualitatively change the results. By comparison, about 50% of the solar flux is absorbed at the surface on Earth (cf. Houghton 1977), about 8–30% estimated on Titan (Samuelson 1983, McKay *et al.* 1989), and about 2.5% on Venus (Tomasko *et al.* 1980). A similar experiment was carried out by Williams (1988b), but only at a 64-day rotation period. That model differs from ours in two important ways: (i) Its absence of convective momentum mixing removes a major source of dissipation and thereby minimizes the important distinction between flows heated from above and below. (ii) The use of a 120° sector model in the absence of a diurnal cycle eliminates zonal wavenumbers 1 and 2, which dominate the eddy kinetic energy spectrum and barotropic conversion at slow rotation rates (cf. Fig. 6 and Table 2 of Del Genio and Suozzo 1987).

We present results for six simulations in which rotation rate, radiative heating profile, surface drag, and stratospheric drag are varied (Table I). Experiments T1–T4 are all run at Titan's presumed rotation period. T1 and T2 differ only in the presence or absence of the stabilizing cloud. T3 and T4 test the effects of removing the stratospheric drag and weakening the surface drag, respec-

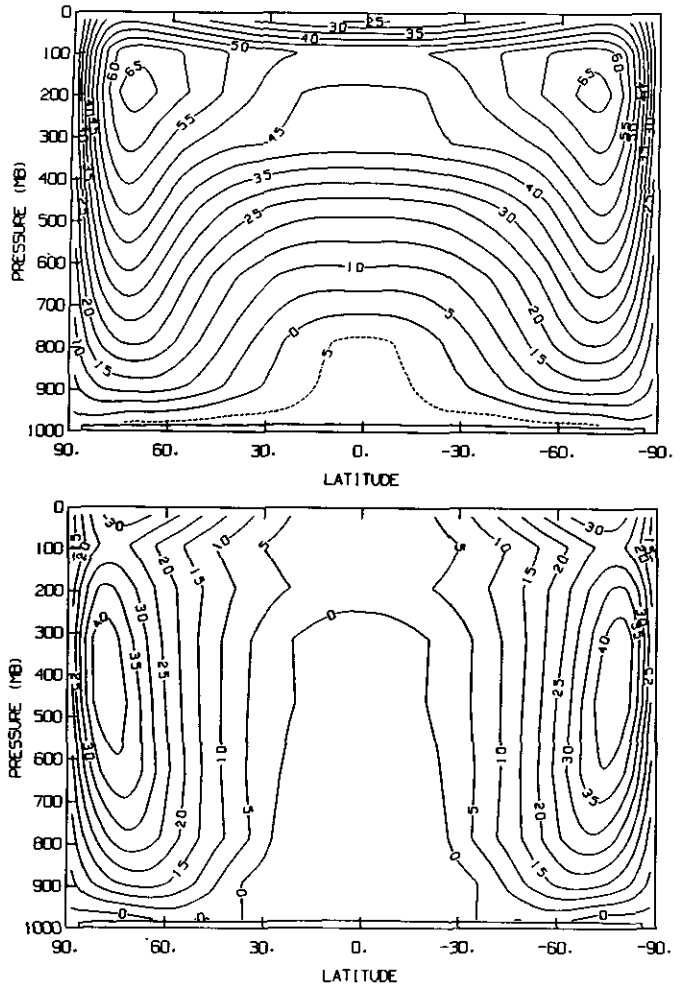

FIG. 1. Zonal-mean time-mean distributions of zonal wind speed (m sec^{-1}) at Titan's rotation period for simulations with (Experiment T1, upper) and without (Experiment T2, lower) an upper troposphere cloud layer.

tively. Experiment V is identical to T3 except that it is run at Venus' rotation period, while Experiment E differs from T1 only by virtue of its being run at Earth's rotation period.

3. CIRCULATION, HEATING, AND STRUCTURE

The temporally and zonally averaged zonal wind field for Experiments T1 and T2 are compared in Fig. 1. Experiment T1 (Fig. 1, upper), which includes the cloud layer, produces a strongly superrotating wind field at most altitudes, with prograde (in the direction of rotation) equatorial winds of nearly 50 m sec^{-1} at the cloud top and weak jets of speed >60 m sec^{-1} near 70° latitude in either hemisphere. The globally integrated angular momentum of the circulation is 2.0 times that corresponding to solid body rotation. The only subrotating winds are near the surface; these are required to transfer angular momentum from the solid planet into the atmosphere.[1]

The latitudinal profile of zonal wind u is intermediate between the uniform angular velocity limit u_ω corresponding to maximum efficiency of the Gierasch mechanism and the uniform angular momentum limit u_m resulting from pure advection by the poleward branch of the Hadley cell (cf. Held and Hou 1980), where

$$u_\omega = u_0 \cos\theta \tag{1}$$

and

$$u_m = \frac{\Omega a \sin^2\theta + u_0}{\cos\theta}. \tag{2}$$

In (1) and (2) u_0 is the equatorial zonal wind speed, Ω the planetary angular velocity, a the planetary radius, and θ the latitude. At $\theta = 70°$ and 200 mbar, for example, in the core of the jet, $u = 67$ m sec^{-1}, whereas $u_\omega = 15$ m sec^{-1} and $u_m = 202$ m sec^{-1}.

The mass-weighted vertically integrated specific absolute angular momentum M of the simulated zonal wind distribution in T1 varies latitudinally approximately as cos θ up to the jet latitude, while absolute vorticity (relative plus planetary) varies approximately as tan θ. By comparison, absolute vorticity would be constant with latitude if $u = u_m$. Since $M = (u + \Omega a \cos\theta)\, a \cos\theta$, cosine variation of M implies that

$$(u + \Omega a \cos\theta)\, a \cos\theta = [(u_0 + \Omega a)a] \cos\theta. \tag{3}$$

The corresponding zonal wind profile is given by

$$u = u_l = u_0 + \Omega a(1 - \cos\theta). \tag{4}$$

This profile corresponds to uniform absolute *linear* momentum, i.e., the sum of the wind speed and planetary rotation speed $u + \Omega a \cos\theta$ is invariant with latitude.

[1] There is no transition to surface westerlies at high latitudes, i.e., the global mean surface torque is nonzero; this is required to balance the momentum sink at the upper boundary due to stratospheric drag and, to a much lesser extent, to the slight internal loss of momentum by the numerics. A model extending to lower pressures with a conservative gravity wave drag scheme and perfect numerics would yield a surface wind pattern with zero torque instead.

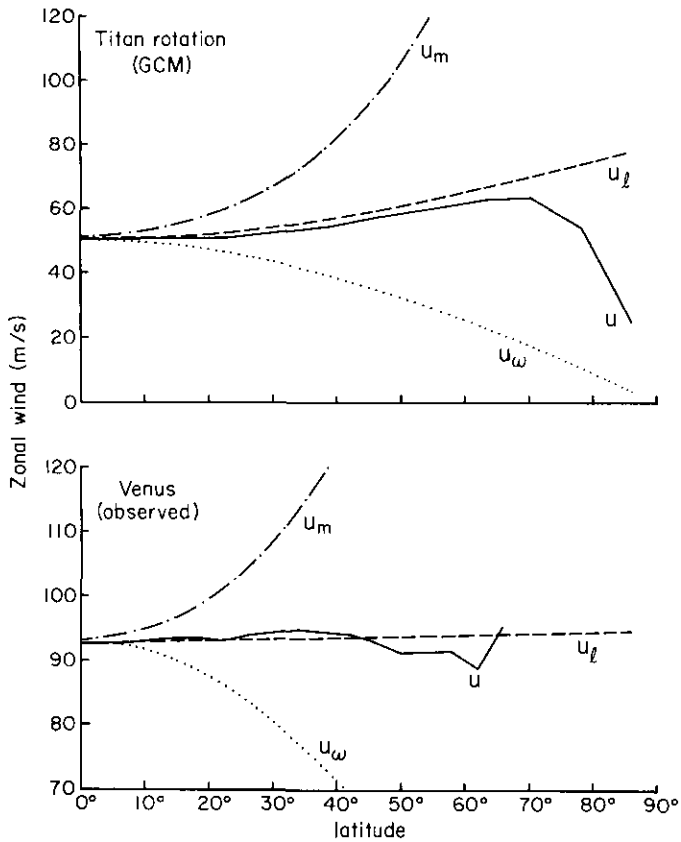

FIG. 2. Latitudinal profiles of time-mean zonal-mean zonal wind (u, solid curves) at 100 mbar in Experiment T1 (upper) and observed at the Venus cloud tops (lower, adapted from Rossow *et al.* 1990) compared to idealized profiles corresopnding to uniform angular momentum (u_m, dash–dot curves), uniform angular velocity (u_ω, dotted curves), and uniform linear momentum (u_ℓ, dashed curves).

Figure 2 shows that this is an excellent approximation to both the jet level winds in the GCM at Titan's rotation period and the observed cloud top zonal winds on Venus (Rossow *et al.* 1990). Although (4) represents an empirical fit to the GCM results, it can also be shown to represent a fundamental constraint on certain types of slowly rotating flows (see Section 5 and Allison and Del Genio 1992 for further discussion).

On the other hand, experiment T2 (Fig. 1, lower), in which the cloud is absent, exhibits only very weak equatorial superrotation (peak $u_0 = 2.2$ m sec^{-1}) and subrotating winds throughout most of the equatorial atmosphere. Substantial jets ($u = 43$ m sec^{-1}) are still present in this experiment, but at higher latitude (78°) and pressure (400 mbar) than in the simulation with the cloud. The poleward shift of the jet is consistent with the slower atmospheric rotation rate (Del Genio and Suozzo 1987). The latitudinal profile is closer, but not identical, to the angular momentum conserving profile ($u = 0.5$–$0.7\ u_m$ in midlatitudes). The globally integrated angular momentum is only 20% higher than would be the case if the atmosphere corotated with the solid planet. This experiment is similar to most of the slow rotation GCM results reported previously.

The corresponding streamfunctions of the mean meridional circulation are shown in Fig. 3. With the cloud (Fig. 3, upper), a two-tiered circulation occurs, with cloud layer and surface Hadley cells separated by a midtropospheric region of weak meridional circulation. Peak poleward/equatorward winds are 2.7/1.5 m sec^{-1} and 5.0/7.9 m sec^{-1} in the cloud layer and surface cells, respectively, but <1 m sec^{-1} in the middle troposphere. Without the cloud (Fig. 3, lower), a single strong surface Hadley cell develops, penetrating only to the 400-mbar level. In both cases the Hadley cell streamfunctions extend to the pole, so that their poleward boundaries are not precisely colocated with the jets. However, the strength of the Hadley cell is negligible poleward of the jet.

The radiative heating/cooling rates which drive the

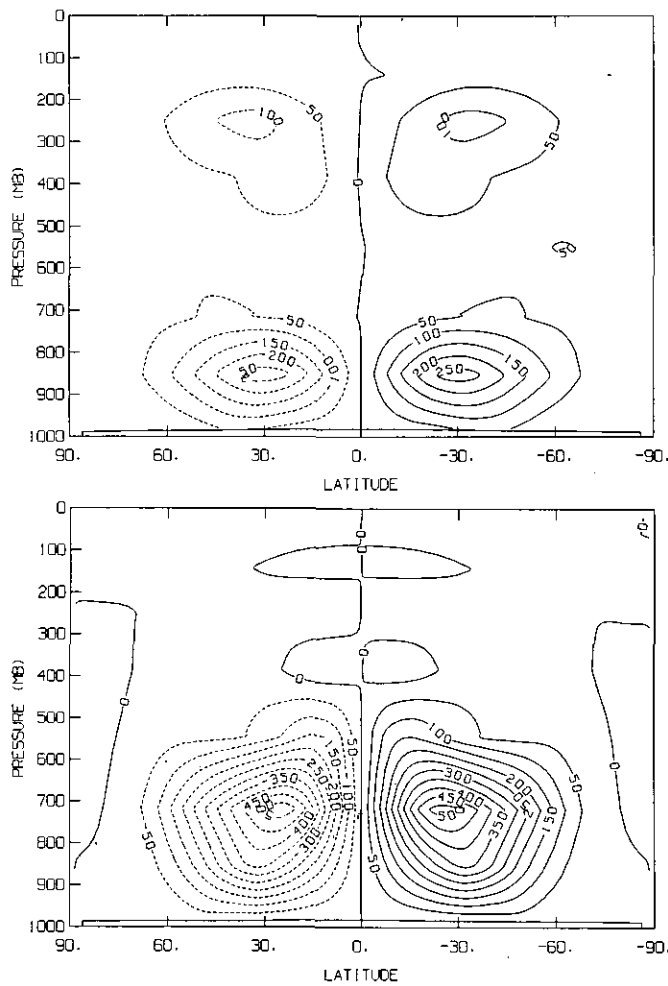

FIG. 3. As in Fig. 1 but for the streamfunction of the mean meridional circulation (10^9 kg sec^{-1}).

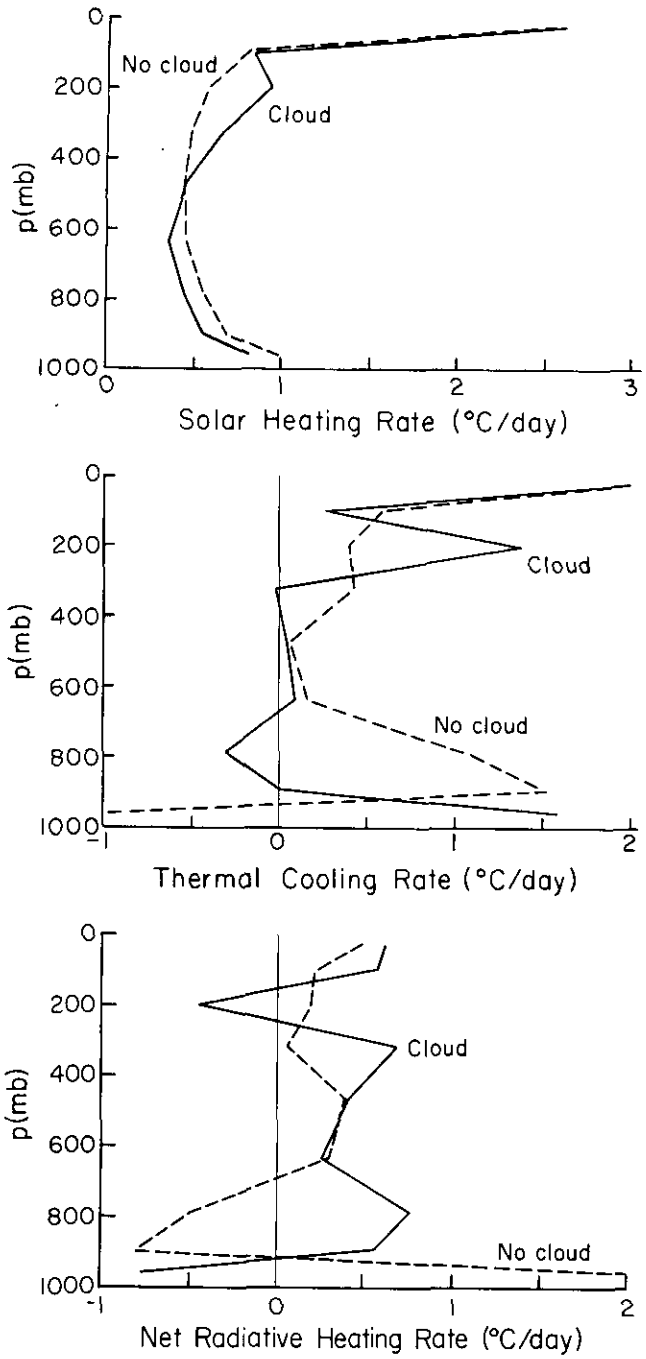

FIG. 4. Vertical profiles of solar (upper), thermal (middle), and net (lower) radiative heating/cooling rates at the equator for experiments with (T1) and without (T2) an upper troposphere cloud layer. For comparison with Fig. 6, 1°C day^{-1} equals approximately 400 × 10^{13} W per unit sigma interval.

mean meridional circulation are shown in Fig. 4. Both solar heating and thermal cooling are amplified at the cloud top level in the cloudy version of the model relative to the model with no cloud. The thermal cooling rate within and near the base of the cloud is near zero. In the version with no cloud, solar heating and thermal cooling are larger in the lower troposphere than in the cloudy version except in the lowest layer, where the warmer surface of the clear model and the large surface–air temperature discontinuity forced by the model's fixed drag coefficient cause a local thermal flux convergence. The net radiative heating profile in the presence of cloud is double peaked in the troposphere, providing the diabatic forcing for the separate surface and cloud layer Hadley cells in Fig. 3 (top). Without the cloud, net radiative heating in the lowest model layer dominates that in the upper troposphere, forcing a single strong lower troposphere Hadley cell (Fig. 3, bottom). The near-surface radiative heating in the clear model is enhanced by turbulent surface sensible heat fluxes which warm the lowest layer at the equator by 5°C day^{-1}, as opposed to only 3°C day^{-1} in the cloudy case.

The thermal structure and dry convective adjustment patterns resulting from the diabatic forcing and dynamical transports in the two simulations are shown in Figs. 5 and 6. A nearly adiabatic convective boundary layer exists in the tropics in T1 (Figs. 5 and 6, upper), but its depth is only 130 mbar. A separate neutrally stable convective layer exists within the upper half of the cloud in low latitudes. These layers are separated by a statically stable region from 350–850 mbar. This structure qualitatively mimics aspects of the observed temperature structure on Venus. In T2 (Figs. 5 and 6, lower), the convective boundary layer is much deeper, extending up to about 600 mbar, with monotonically increasing static stability above. Because convective adjustment also mixes momentum, the convective layers are also locations of kinetic energy dissipation in the model.

The meridional potential temperature gradient $\partial\Theta/\partial y$ is diagnostic of the effects of the general circulation, with small gradients at lower latitudes controlled by Hadley cell heat transport and large gradients in a baroclinic zone at higher latitudes. (Near-surface air, which more closely follows the surface energy fluxes, is the exception.) From this point of view, the *effective* extent of the Hadley cell (as opposed to that defined by the streamfunction) is inversely proportional to superrotation strength: above the boundary layer, the region of small $\partial\Theta/\partial y$ is much greater in T2 than in T1 and, in T1, the width of this region shrinks as we move from the lower to upper troposphere.

The sensitivity of superrotation to stratospheric drag, surface drag, and rotation rate is demonstrated in Fig. 7, which shows the zonally averaged zonal wind fields for the other four simulations. Experiment T3 (Fig. 7a) is identical to T1 except that stratospheric drag, a strong kinetic energy sink, is removed. The result is an even stronger, more uniform superrotation at all altitudes, increasing monotonically to equatorial wind speeds >110 m

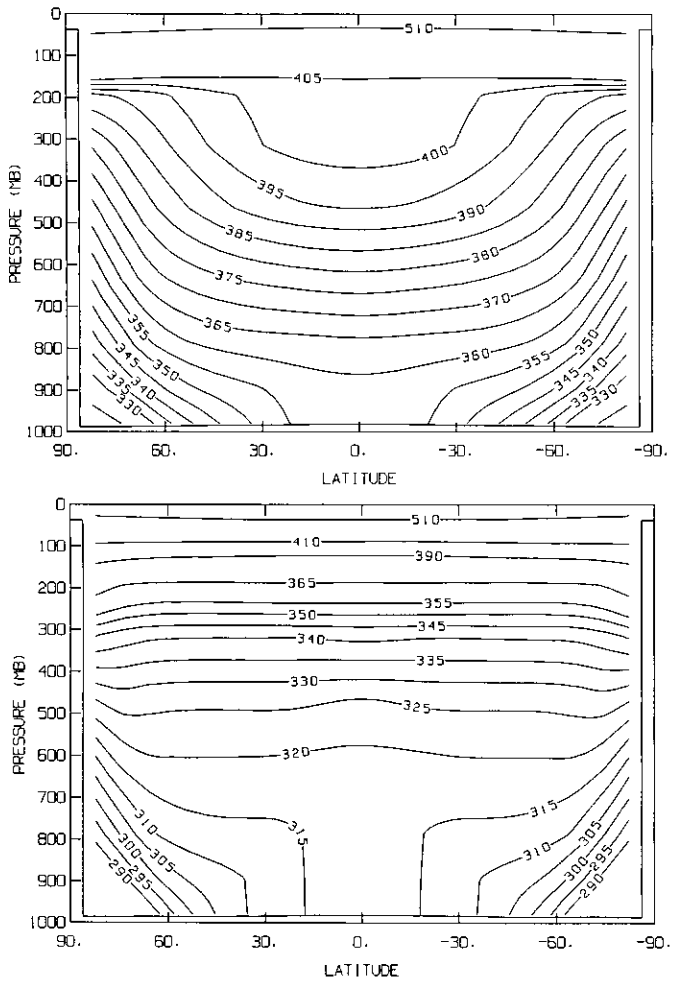

FIG. 5. As in Fig. 1 but for potential temperature (K).

sec^{-1} in the highest model level (27 mbar). The angular momentum in this run is 3.0 times greater than that corresponding to solid body corotation. Weakening the surface drag by an order of magnitude (Experiment T4, Fig. 7b) has the opposite effect, because it reduces the efficiency of angular momentum transfer from planet to atmosphere. Superrotation still occurs, but with peak equatorial winds of only 12 m sec^{-1} and distinct high latitude jets. Global angular momentum is only 30% higher than for a corotating atmosphere, much closer to that for the cloudless atmosphere. This result emphasizes the fact that knowledge of the nature of Titan's surface (i.e., fractional ocean vs land coverage, topography) is crucial to an understanding of its atmospheric dynamics.

Experiment V (Fig. 7c) is identical to T3 except that it uses Venus' rotation period rather than Titan's. Since the rotation rates of these planets differ by a factor of 15, one might expect the absolute magnitude of superrotation to be somewhat less in V than in T3, and this is indeed the case. Relative to the solid planet, though, V superrotates more efficiently than T3: its global angular momentum is 3.5 times that corresponding to corotation with the surface. What is most surprising is that the vertical profile of zonal wind is completely different in the two experiments. Experiment T3 is characterized by relatively uniform vertical shear. Experiment V, on the other hand, exhibits strong equatorial zonal winds in the uppermost model layer (64 m sec^{-1}), but superrotation is effectively absent within and below the cloud except for weak (7–8 m sec^{-1}) cloud level high-latitude jets. This must be considered an unsuccessful simulation of superrotation because the effect of the upper boundary condition of the GCM is potentially important when stratospheric drag is removed. One possible explanation for the lack of superrotation at lower altitudes is the GCM's shallow depth (3.6 scale heights at the top model level, 1.6 at cloud top) relative to the actual depth of superrotating flow on Venus (about 7 scale heights). In Gierasch's (1975) theory, the magnitude of superrotation scales exponentially with the depth

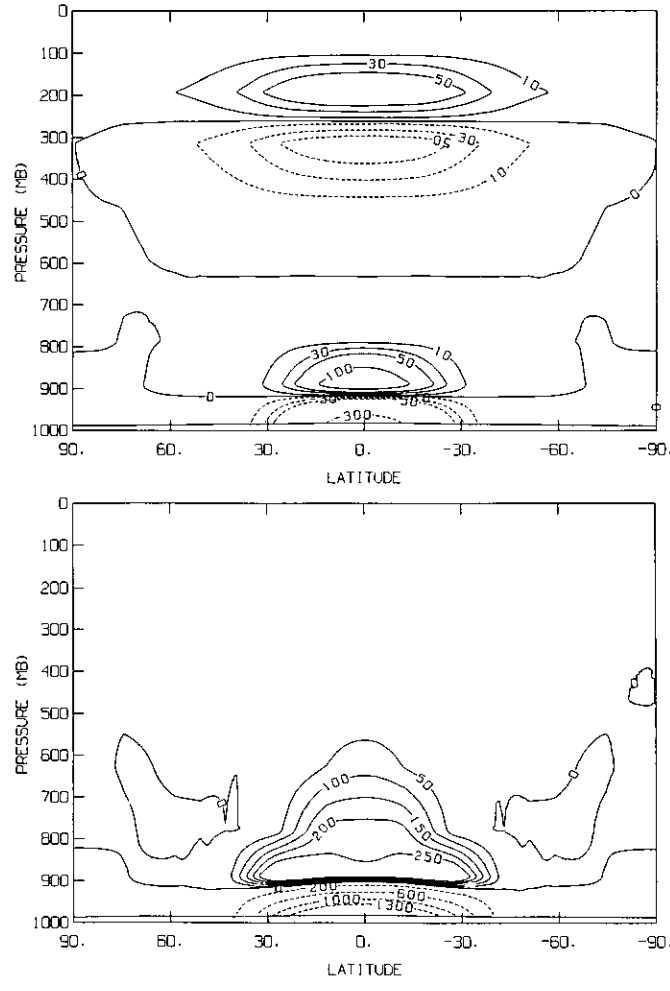

FIG. 6. As in Fig. 1 but for the heating/cooling rate by dry convective adjustment (10^{13} W per unit sigma interval).

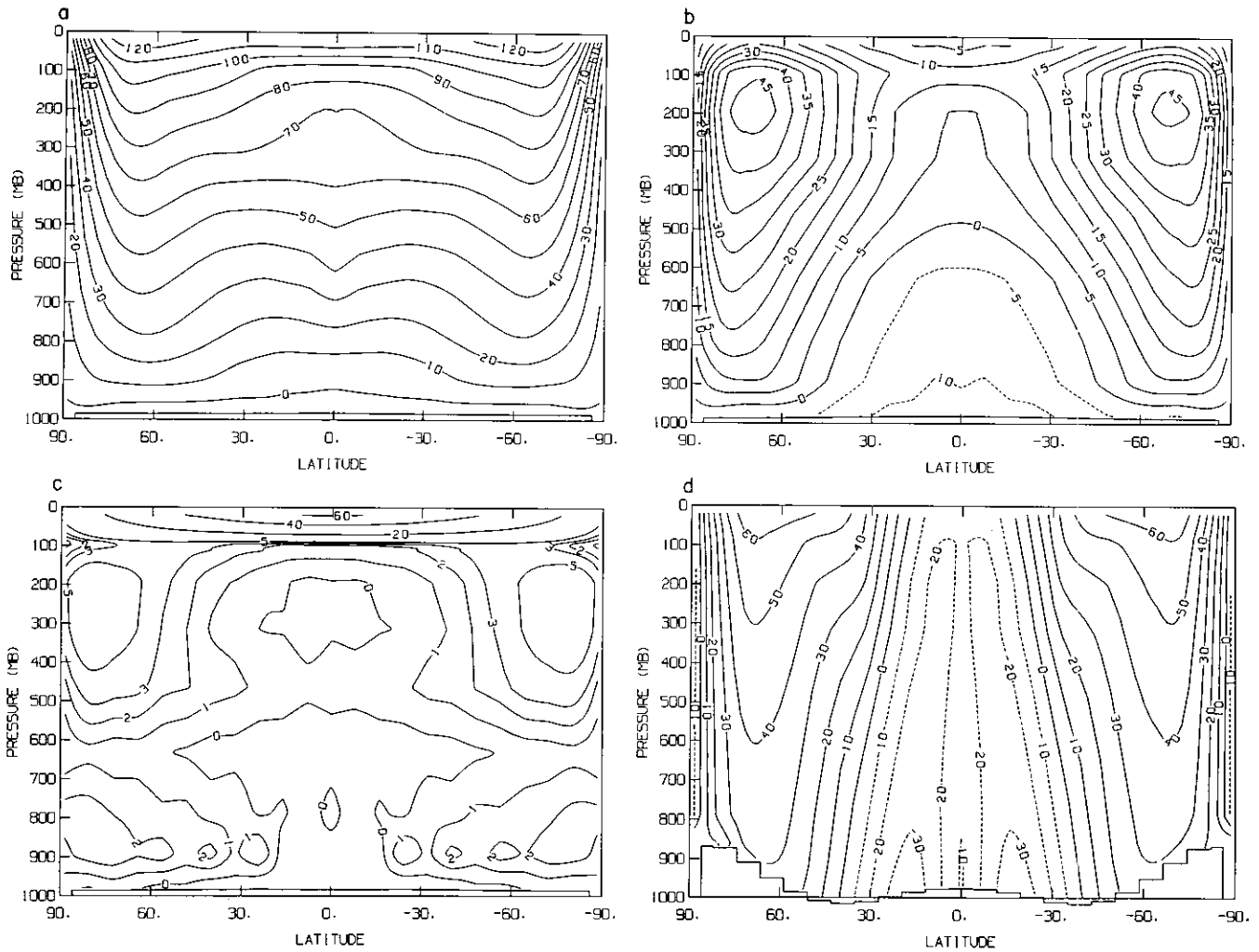

FIG. 7. Zonal-mean zonal-wind fields (m sec^{-1}) for Experiments (a) T3, (b) T4, (c) V, and (d) E. Termination of contours near the surface in E is a result of the large latitudinal variations in surface pressure in this simulation.

of the flow in scale heights. Another possible reason is the absence of thermal tides or gravity waves which might act to redistribute angular momentum vertically. In the context of these experiments, however, the difference between V and T3 can be traced to the effect of rotation on meridional heat transport and convection; we will return to this point in the next section.

Experiment E (Fig. 7d) illustrates that equatorial superrotation by the mechanism discussed in this paper is unique to the slowly rotating dynamical regime. At Earth's rotation period, the effect of a stabilizing cloud is simply to amplify the observed features of Earth's general circulation, with strong subrotating "trade winds" at low latitudes and strong superrotating jets displaced poleward from their observed location. (The GCM accurately simulates the jet location and magnitude when forced with realistic diabatic heating for Earth; see Fig. 29 in Hansen *et al.* 1983).

4. MOMENTUM BALANCE AND ENERGETICS

To diagnose the processes responsible for the presence or absence of superrotation, we analyze the momentum and energy budgets of the various simulations. Figure 8 shows the angular momentum transports for the mean meridional circulation and large-scale eddies in Experiment T1. Hadley cell transport is poleward and upward in each cell up to cloud top (Figs. 8a and 8c), as it must be if angular momentum increases with height and decreases with latitude (Gierasch 1975). Horizontal eddy momentum fluxes are strongly equatorward in both hemispheres at all altitudes except near the surface (Fig. 8b). Eddy kinetic energy peaks in the vicinity of the jets. The mean amplitude of the eddies is 10–15 m sec^{-1}, with about half the total eddy kinetic energy occurring at zonal wavenumber 1. Averaged globally the eddy transport is 90% as large as the Hadley cell transport, because of partial cancellation

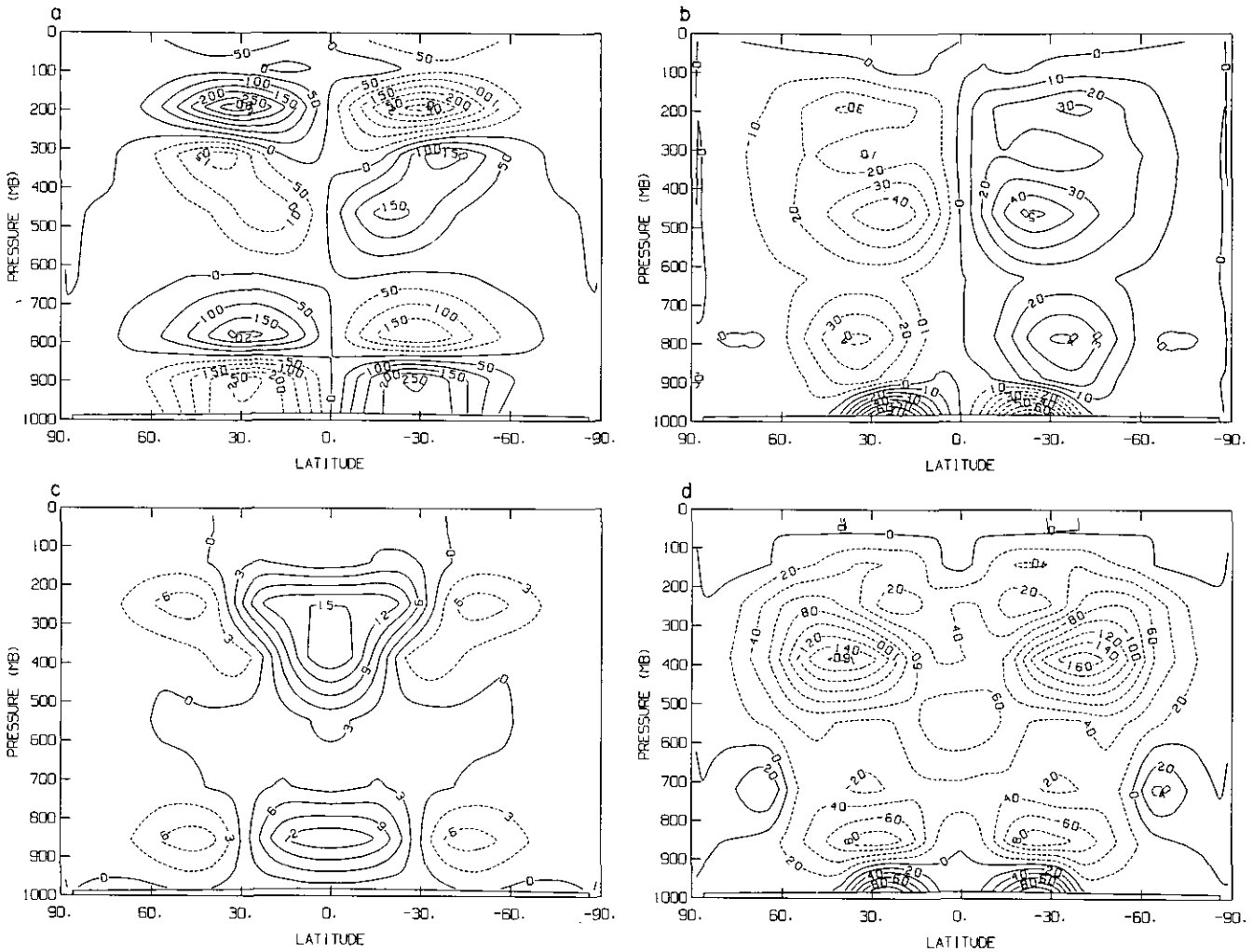

FIG. 8. Zonal-mean angular-momentum transports in Experiment T1: northward transport (a) by the mean meridional circulation (10^{18} J) and (b) by eddies (10^{18} J), and vertical transport (c) by the mean meridional circulation (10^{18} J) and (d) by eddies (10^{16} J).

between the poleward and equatorward Hadley cell branches. Thus, the eddies provide fairly efficient vorticity mixing. Upward Hadley cell transport is balanced both by downward large-scale eddy fluxes (Fig. 8d) and convective momentum mixing (not shown), with convergence by the former dominating in the lower troposphere and by the latter in the cloud layer.

In Experiment T2, on the other hand, Hadley cell transport extends only up to 400 mbar, with weak contributions above (Figs. 9a and 9c). Fairly strong equatorward eddy momentum fluxes still exist in the middle and lower troposphere (Fig. 9b), but they are colocated with convective fluxes (cf. Fig. 6, lower) which dissipate kinetic energy themselves and mix momentum downward so that energy may be further dissipated by surface drag. In the upper troposphere, eddy momentum fluxes are only weakly equatorward at low latitudes and actually poleward at higher latitudes, eliminating any chance for superrotation. Globally averaged, eddy-momentum fluxes in T2 are only 40% as large as the Hadley cell transport.

The direction and location of the eddy momentum fluxes of T1 (away from the jet maximum at latitudes of strong meridional shear), along with the mixing of absolute vorticity at middle latitudes, argues that the eddies responsible are the product of barotropic instability of the jet (Kuo 1949, 1978). If this is the case, we should expect weak associated eddy heat transports. Figure 10 demonstrates that this is indeed the case; globally averaged horizontal transport of dry static energy (sensible heat plus geopotential energy) by large-scale eddies is only 13% of the total by the general circulation, most of it occurring near the surface. Within the cloud layer, eddy heat transport is effectively nonexistent, representing only 2% of the total transport.

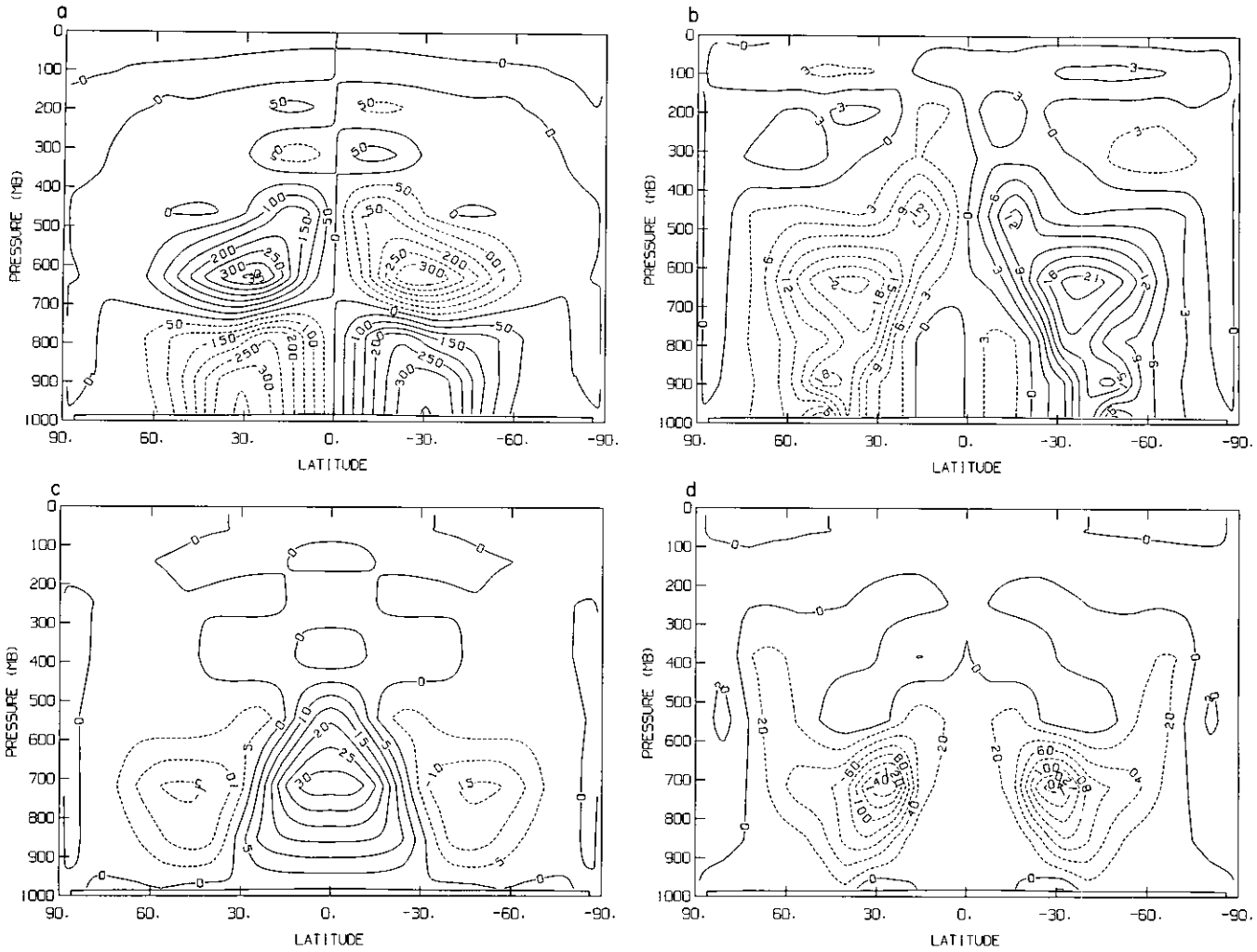

FIG. 9. As in Fig. 8, but for Experiment T2.

Note that the presence of barotropic instability cannot be inferred directly from the evolved mean flow, which adjusts to neutrality on a time scale comparable to that of the Hadley cell forcing. During the spinup phase, the poleward branch of the Hadley circulation creates uniform zero absolute vorticity up to the jet latitude, with sharply increasing vorticity magnitude poleward of the jet where the planetary vorticity dominates. Perturbations then cause local absolute vorticity extrema which are barotropically unstable. The resulting horizontal mixing produces the observed tan θ profile of absolute vorticity, which approaches neutral stability near the equator.

The eddy properties in the slowly rotating dynamical regime are quite different from those in the terrestrial baroclinic regime (Fig. 11). In experiment E, eddy heat fluxes are poleward (Fig. 11, upper) as in Experiment T1, but they account for 60% of the total horizontal heat transport by the general circulation. The horizontal eddy momentum transport in E is poleward at most altitudes in both hemispheres (Fig. 11, lower), exactly the opposite of that required to maintain an equatorial superrotation. These properties are characteristic of baroclinically unstable waves, and they explain the presence of equatorial subrotation at the terrestrial rotation rate.

The small eddy heat transports in the slowly rotating regime do not by themselves necessarily demonstrate the nature of the eddies that produce them, because the transports are also a result of the small meridional potential temperature gradients at the latitudes of peak transport. For a more definitive assessment, we estimate effective horizontal diffusivities of heat (κ_h) and momentum (ν_h) as the ratio of the eddy flux to the meridional gradient of the quantity transported. We then define an effective Prandtl number,

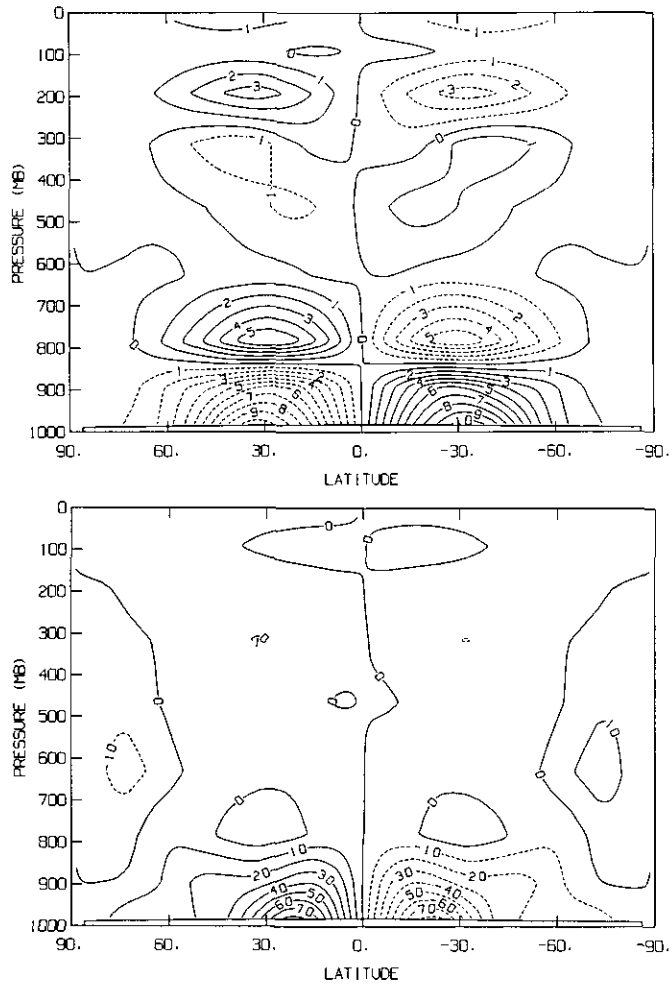

FIG. 10. Northward transport of dry static energy by the mean meridional circulation (10^{17} W, upper) and by eddies (10^{14} W, lower) in Experiment T1.

$$\mathrm{Pr} = \frac{\nu_h}{\kappa_h} = \frac{|F_M|\,\Delta s}{|F_s|\,\Delta M}, \tag{5}$$

where F_M and F_s are the peak zonally and vertically integrated eddy transports of absolute angular momentum (M) and dry static energy (s), respectively, and Δs and ΔM are the equator–pole differences in these quantities. (Gierasch's 1975 theory assumes diffusion of angular velocity, but the resulting diffusivity is approximately the same as that in (5) if the fluxes are evaluated in midlatitudes.) In Experiment E, Pr = 0.2, consistent with the interpretation as baroclinic eddies whose primary role is to transport heat. In Experiment T2, Pr = 0.3, indicating only slightly more barotropic behavior. In the most highly superrotating experiments (T1 and T3), on the other hand, Pr = 2.8 and 4.1, respectively, attesting to the more barotropic character of the eddies in these cases. It is noteworthy, though, that in none of the experiments do we find extremely large Prandtl numbers. In Gierasch (1975), by comparison, Pr = ∞ is assumed: We will return to this point in Section 5.

The conditions necessary for strong superrotation are perhaps most conveniently summarized by examining the components of the energy cycle (Fig. 12). In all the slow rotation simulations energy flows as follows: (i) Radiative heating/cooling (G) generates available potential energy (A) by establishing an equator–pole temperature gradient. (ii) The mean meridional circulation converts A to kinetic energy of the mean zonal flow (K_Z) via the angular momentum transport of the poleward branch of the Hadley cell, which establishes the high-latitude jets. (iii) K_Z is either converted to eddy kinetic energy (K_E) by barotropic instability or dissipated (D_Z) by convective momentum mixing, surface drag, or stratospheric drag. (iv) K_E is converted back to A by vertical eddy heat transports (not shown), which are downward everywhere except above

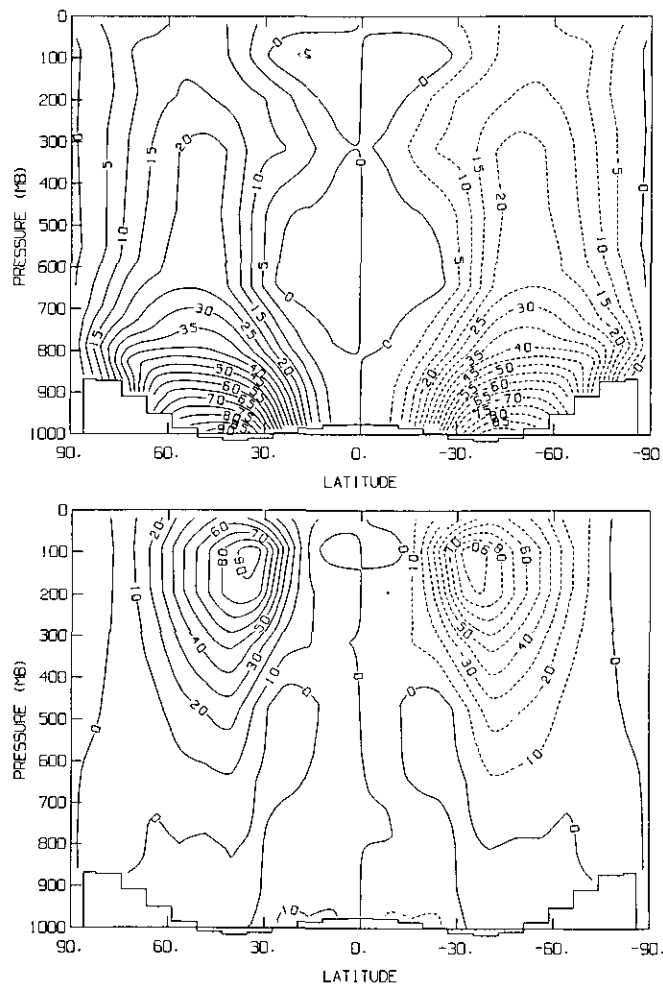

FIG. 11. Northward eddy transports of dry static energy (10^{14} W, upper) and angular momentum (10^{18} J, lower) in Experiment E.

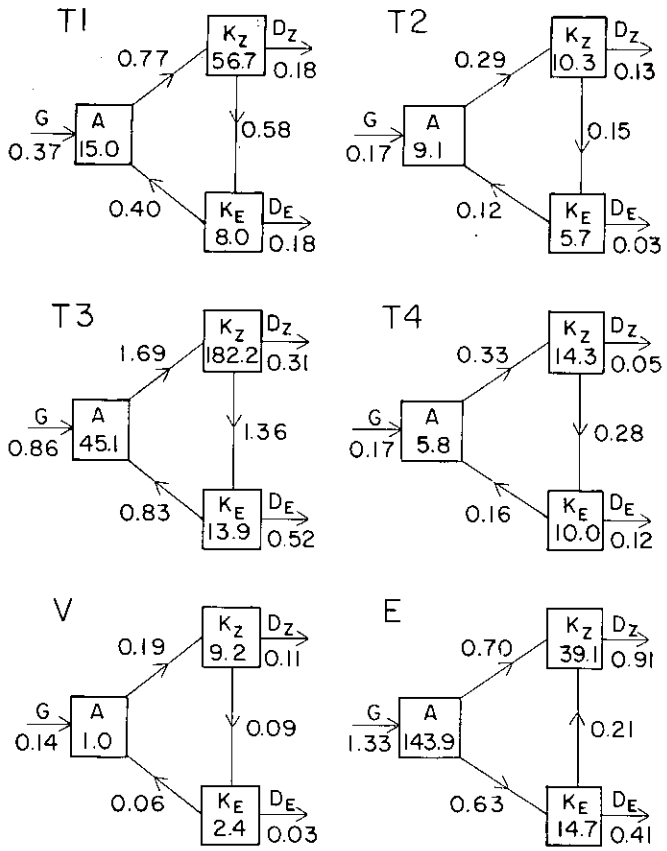

FIG. 12. Atmospheric energy cycle for each of the six simulations. Available potential energy (A), zonal mean kinetic energy (K_Z), and eddy kinetic energy (K_E) in 10^5 J m^{-2}; generation of A (G), dissipation of K_Z (D_Z) and K_E (D_E), and conversions between energy forms (indicated by connecting arrows) in W m^{-2}.

the cloud top. This type of energy cycle is just the opposite of that which characterizes Earth's troposphere. In Experiment E, for example, baroclinic eddies convert A to K_E and then K_E to K_Z. (A is converted to K_Z in this experiment because of the strong Hadley cell forcing by the cloud; on Earth, midlatitude Ferrel cell conversion of K_Z to A is thought to slightly outweigh the effect of the Hadley cell; Houghton 1977.)

The key to superrotation can be found by comparing the two possible sinks for K_Z in the strongly superrotating (T1, T3) and nonsuperrotating (T2) Titan rotation cases. When barotropic conversion (C_{ZE}) dominates dissipation, strong superrotation results; when dissipation dominates, zonal winds are weak. In T1, $C_{ZE}/D_Z \approx 3$, because convection is restricted to isolated layers; it is even larger in T3 because of the absence of stratospheric drag. In T2, however, $C_{ZE} \approx D_Z$, because convective fluxes are stronger and the eddies flux momentum into the region of boundary layer convection. This appears to have been the weakness of all previous attempts to produce superrotation in slowly rotating GCMs. The GCM results are consistent with the two-dimensional simulations of Rossow and Williams (1979), in which significant modification of a forced jet structure by barotropically unstable eddies occurs only when the dissipation time scale exceeds the dynamical time scale for the nonlinear eddy processes. T4 is a special case; C_{ZE} exceeds D_Z by a factor of 6 in this experiment, yet equatorial winds are relatively modest because the weak surface drag limits the transfer of angular momentum from solid planet to atmosphere. In this case, it is the source rather than the sink process that limits superrotation.

Further evidence of the controlling effect of static stability comes from examination of Experiment V. At Venus' rotation rate, the direction of the energy cycle is similar to that at Titan's rotation rate, and the solar heating distribution is essentially identical as well because of the prescribed cloud, yet strong superrotation occurs only at the highest model level. However, Fig. 12 shows that despite the similar solar forcing in V, T1, and T3, dissipation of K_Z is comparable to barotropic conversion in Experiment V.

The difference between the Venus and Titan cases lies in the effect of rotation on the mean meridional circulation. For the zonally averaged flow, the thermodynamic energy equation for Hadley cells stretching from equator to pole can be scaled as

$$\frac{V}{a}\Delta_h + \frac{W}{D}\Delta_v = Q, \tag{6}$$

where V and W are the mean meridional and vertical velocity scales, D is the total depth of the circulation, Δ_h and Δ_v are the meridional and vertical potential temperature contrasts, and Q is the diabatic heating rate. Continuity implies that $V/a \sim W/D$, so if $\Delta_h \ll \Delta_v$,

$$V \sim \frac{Qa}{\Delta_h + \Delta_v} \sim \frac{Qa}{\Delta_v}\left(1 - \frac{\Delta_h}{\Delta_v}\right). \tag{7}$$

Globally averaged, $\Delta_v \approx 64$–68 K is almost independent of rotation rate in the GCM, while $\Delta_h = 4$, 24, and 55 K in Experiments V, T1, and T3, respectively. The smaller Δ_h at Venus' rotation rate implies a larger V in (7), i.e., a more vigorous Hadley circulation.

Figure 13 shows the resulting effects on the dynamics. The Hadley cell in the cloud layer is much stronger in Experiment V (Fig. 13a) than in Experiment T3, and its heat transport twice as large, leading to nearly horizontal isentropes (Fig. 13b). Associated with this, convective mixing, which is restricted to low latitudes away from the jet at Titan's rotation (Fig. 6a), extends all the way to the pole at Venus' rotation (Fig. 13c). Thus, despite the

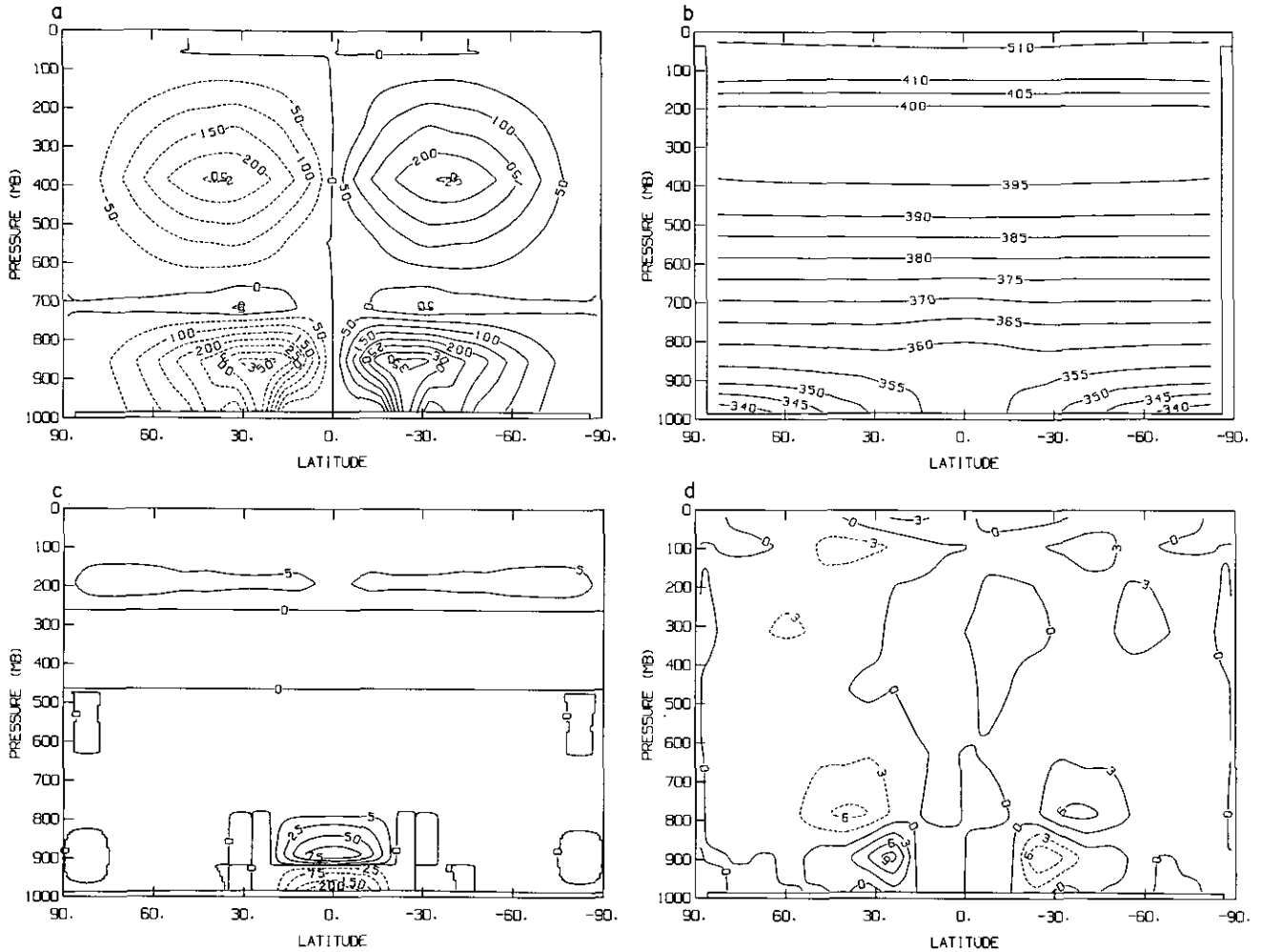

FIG. 13. (a) Streamfunction of the mean meridional circulation (10^9 kg sec^{-1}), (b) potential temperature (K), (c) dry convective heating (10^{13} W per unit sigma interval), and (d) northward eddy angular-momentum transport (10^{18} J) for the experiment at Venus' rotation period (V).

presence of generally equatorward eddy momentum fluxes (Fig. 13d), convective dissipation within the jet region limits the extent of barotropic conversion and prevents superrotation in the cloud. It is worth noting in this regard that the observed cloud morphology on Venus tentatively suggests that cloud-layer convection (if the presence of mesoscale cellular features in ultraviolet images is an indication) is restricted to latitudes between ±40° (Del Genio and Rossow 1982).

In principle, boundary layer convective momentum mixing and surface drag can also provide the excessive dissipation which inhibits superrotation in V. We performed a sensitivity test using a τ = 120 cloud which completely shuts off boundary layer convection but enhances cloud layer convection. Equatorial winds in the cloud layer increased only to 3–4 m sec^{-1} with no other significant changes. Another sensitivity test with C_D decreased by an order of magnitude reduced the peak wind in the top layer to 40 m sec^{-1} and produced subrotating winds of 1–2 m sec^{-1} in the cloud layer. Thus, surface effects do not appear to be the primary impediment to superrotation in V.

5. DISCUSSION

a. Have the Gierasch–Rossow–Williams Conditions for Superrotation Been Met?

Gierasch's (1975) theory first required that the flow be in cyclostrophic balance and that Ri $\gg h$, where Ri is the Richardson number (Ri = Δ_v/Δ_h for cyclostrophic scaling) and h is the dimensionless depth of the flow in scale heights ($h \approx 2$ in the GCM). In Experiment V, $\Delta_v/\Delta_h \approx 16$, so vertical heat advection dominates meridional advection but the flow is too weak at most levels to be in cyclostrophic balance. At Titan's rotation period, the Coriolis force is not negligible; since $\Delta_v/\Delta_h \approx 3$ in the

global mean in Experiment T1, horizontal heat transport plays a role (horizontal temperature contrasts are much smaller, though, in the cloud layer). The flow is nearly in *gradient* wind balance with the presure field (see Fig. 14 and discussion below). These conditions affect only the scaling, however, not the basics of the mechanism.

The essence of the Gierasch mechanism is that (i) Hadley cell horizontal heat transport must dominate eddy horizontal heat transport, (ii) equatorward eddy angular momentum transport must dominate poleward Hadley cell angular momentum transport, and (iii) vertical eddy angular momentum transport must be weak relative to horizontal eddy angular momentum transport. Rossow and Williams' (1979) two-dimensional simulations suggest that the above conditions will be realized only in a weakly forced flow, i.e., one in which the nonlinear kinetic energy cascade processes dominate the forcing and drag processes. The horizontal and vertical diffusivities of angular momentum (ν_h, ν_v) and heat (κ_h, κ_v) in Experiment T1, estimated from the simulated eddy fluxes (including convection) and gradients of the zonal and time mean fields, are

$$\begin{aligned} \nu_h &\approx 3 \times 10^6 \text{ m}^2 \text{ sec}^{-1}, \\ \nu_v &\approx 15 \text{ m}^2 \text{ sec}^{-1}, \\ \kappa_h &\approx 1 \times 10^6 \text{ m}^2 \text{ sec}^{-1}, \\ \kappa_v &\approx 7 \text{ m}^2 \text{ sec}^{-1}. \end{aligned} \tag{8}$$

For the poleward branch of the Hadley cells in T1, V $\approx$ 1.1 m sec^{-1} Thus, the ratio of eddy to Hadley cell horizontal heat transport is $\kappa_h/Va \approx 0.1$, which satisfies the first Gierasch criterion. The ratio of eddy to Hadley cell horizontal angular momentum transport is $\nu_h/Va \approx 0.4$, which does not satisfy the Gierasch requirement. Finally, the ratio of vertical to horizontal eddy angular momentum transport can be expressed as $(\nu_v/\nu_h)(a/D)^2 \approx 0.6$, which only marginally satisfies the criterion. The dominance of barotropic conversion over dissipation in T1 and T3, as opposed to the strong dissipation in T2 and V, is consistent with the Rossow–Williams weak forcing scenario for superrotation.

The discrepancies between the GCM realization and the Gierasch criteria arise because Gierasch considered a parameter setting appropriate to maximum efficiency of his mechanism. Specifically, $\nu_h/Va \gg 1$ and $(\nu_v/\nu_h)(a/D)^2 \ll 1$ are required to produce a uniform angular velocity zonal flow profile. This profile was shown by Rossow and Williams (1979) to be the relaxed state of two-dimensional turbulence and thus the configuration of maximum possible superrotation. The GCM instead finds a middle ground between this extreme and the uniform angular momentum extreme corresponding to Hadley cell dominance and no equatorial superrotation. Given that downward eddy mixing must balance upward Hadley cell transport in the horizontally averaged momentum equation, it must also be true that the vertical and horizontal eddy mixing are comparable in the intermediate regime.

The Gierasch model also assumes that the horizontal Pr = ∞, so that eddy heat transports do not destroy the meridional temperature gradient that gives rise to the Hadley cell and barotropically unstable high latitude jets. Pr does increase from <1 to >1 in the GCM as the rotation rate decreases and from the weakly to strongly superrotating experiments; however, in all cases Pr $<$ O(10). The small eddy heat fluxes we find are attributable more to the small meridional temperature gradients along which the eddies transport than to the purely barotropic character of the eddies themselves. The GCM situation thus more closely resembles the parameter setting envisioned by Mayr and Harris (1983), who showed superrotation solutions of a two-dimensional model for the regime Pr = 1.

The uniform linear momentum latitudinal profile of zonal wind realized by the GCM may reveal a fundamental property of slowly rotating atmospheres. It can be shown that this profile results when the total Ertel potential vorticity on a sphere is well-mixed with respect to the neutral equatorial value for a stable circulation, assuming a moderate Richardson number comparable to that in the numerical simulations (Allison and Del Genio 1992). The potential vorticity constraint for slowly rotating flows is a generalization of the well-known pseudo-potential vorticity condition for neutral stability of baroclinic flows in quasi-geostrophic atmospheres. The GCM winds may therefore represent the fully relaxed state for a *three-dimensional* slowly rotating atmosphere of intermediate stability. This contrasts with the two-dimensional case, in which absolute vorticity mixing yields a uniform angular velocity wind profile in the fully relaxed state (Rossow and Williams 1979).

b. Does Titan Superrotate?

We have established that three conditions are necessary for strong equatorial superrotation by the Gierasch–Rossow–Williams mechanism: (i) The planet must rotate slowly enough so that eddy transports are more barotropic (equatorward momentum flux, small heat flux) than baroclinic (large poleward heat flux, usually with poleward momentum flux) in character; (ii) the diabatic heating profile must suppress vertical mixing, so that the kinetic energy of the mean flow is preferentially converted to eddy kinetic energy as opposed to being dissipated; (iii) surface drag must be strong enough for efficient transfer of angular momentum from planet to atmosphere.

Previous GCM simulations with variable rotation rate suggest that the transition from the baroclinic regime to

the quasi-barotropic regime occurs when the midlatitude Rossby radius of deformation L_d becomes comparable to the size of the planet (cf. Del Genio and Suozzo 1987). The deformation radius is given by $L_d = NH/f$, where N is the Brunt–Väisälä frequency, H the scale height, and $f = 2\Omega \sin\theta$ the Coriolis parameter ($=2^{1/2}\Omega$ at 45° latitude). We therefore expect superrotation on Titan if $L_d > a$, or if the rotation period $P = 2\pi/\Omega$ satisfies

$$P > \frac{2^{3/2}\pi a}{NH}. \tag{9}$$

For Titan, with $a = 2575$ km, $N = 3.3 \times 10^{-3}$ sec^{-1}, and $H = 18$ km (Allison and Travis 1986), the critical rotation period is thus $P = 4.2\,d$. If Titan is tidally locked to Saturn, as is usually assumed, then its rotation period is close to 16 days, which clearly puts it into the quasi-barotropic regime. The absence of longitudinal brightness temperature contrasts in Voyager IRIS observations of Titan, and thermal wind inferences of midlatitude angular momentum 3 times the planetary value, have been interpreted to mean that Titan is in the slowly rotating regime (Flasar *et al.* 1981).

The weakness of vertical mixing on Titan is unfortunately more uncertain. Voyager radio occultation temperature profiles (Lindal *et al.* 1983) are dry adiabatic only up to about 3.5 km altitude and statically stable above, suggesting that dry convective turbulence is confined to a fairly shallow boundary layer. This is consistent with the effect of a planetwide haze on surface insolation. By comparison, Flasar *et al.* (1981) infer a Hadley cell of nearly 50 km depth. However, Flasar (1983a) has shown that Titan's troposphere is likely to be conditionally unstable to deep methane moist convection, which could extend over a significant fraction of the depth of the troposphere. If deep methane cumuli are pervasive, the strength of vertical mixing might be much greater than that suggested by the temperature profile alone, and this could limit the extent of equatorial superrotation. However, momentum transport and energy dissipation by moist convection are more complex than those by dry convection. Furthermore, if the Titan troposphere is substantially subsaturated outside the convecting regions, as is the case in Earth's tropics, the resulting cumulus heating might actually further stabilize the large-scale atmosphere, promoting superrotation instead.

Of course, extensive deep moist convection on Titan requires the existence of a surface source of methane. Initially, it was suggested that Titan might be covered by a mixed ethane–methane ocean (Lunine *et al.* 1983, Flasar 1983b). However, at least some of the radar returns obtained from Titan's surface seem to be inconsistent with an ocean-covered surface (Muhleman *et al.* 1990). Nonetheless, the apparent high relative humidity of near-surface methane on Titan (McKay *et al.* 1989) argues for at least a regional surface source, perhaps in the form of lakes or shallow seas. This suggests that although superrotation is likely on Titan, a situation like that realized in our Experiment T2 cannot yet be ruled out. The absence of a global ocean would also imply that the relevant surface drag coefficient for Titan is significantly greater than the lower limit estimated by Allison (1992), which would rule out a weakly superrotating scenario similar to that in Experiment T4.

The Cassini/Huygens mission should provide much of the data needed to constrain the dynamics of Titan's atmosphere. The Titan Radar Mapper will determine the planet's rotation rate and areal coverage of surface methane sources and may also characterize the surface roughness. The Descent Imager/Spectral Radiometer will determine the solar flux deposition profile that drives the dynamics and the static stability. The Doppler Wind Experiment will directly measure the instantaneous vertical profile of zonal wind at one location; given our results, it is clear that the probe should enter Titan's atmosphere near the equator to maximize the scientific return of this experiment. Although Voyager images showed almost no trackable cloud features, the Cassini Imaging Science Subsystem will include near-infrared channels which may detect tropospheric cloud contrasts and provide a latitudinal profile of zonal and meridional winds. The imaging system will also carry channels for lightning detection as an indicator of deep moist convection.

Zonal wind profiles can also be estimated by vertically integrating the thermal wind equation, assuming negligible surface wind, and using temperatures from the Radio Science Subsystem and Composite Infrared Spectrometer. Figure 14 compares the actual wind in the GCM to a thermal wind estimate based on a direct gradient wind balance (Coriolis plus curvature vs pressure gradient forces). In general, the gradient wind is within 3 m sec^{-1} of the actual zonal wind. The only exceptions are the lowest and highest model layers, where surface and stratospheric drag are non-negligible terms in the momentum balance, and the low-latitude lower troposphere, where there is no gradient wind solution because of a reversal of sign of the latitudinal geopotential gradient (indicating that the momentum balance is dominated by eddy fluxes).

Since the gradient wind equation is quadratic, a second solution corresponding to strong subrotation is possible as well (although the winds are ~10 m sec^{-1} weaker because of competition between the curvature and Coriolis terms). This solution is unlikely if the mechanism taking place in the GCM was responsible for establishing Titan's winds, because the Coriolis torque on the poleward branch of the Hadley cell determines the ultimate wind direction in the spinup phase (cf. Leovy 1973). The situation is analogous to that which constrains the circulation

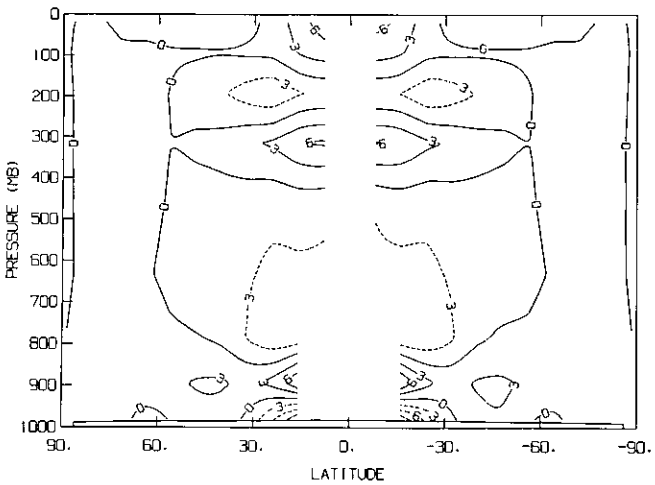

FIG. 14. Difference between the realized zonal mean zonal wind and the gradient wind derived from the geopotential field (m sec^{-1}) for Experiment T1. Missing data at the equator arise from model resolution limits on meridional gradients and, below the 700-mb level, in regions of latitudinally increasing geopotential for which a gradient wind solution does not exist.

direction of terrestrial hurricanes to always be cyclonic. We cannot observe the evolution of Titan's general circulation, only the equilibrium state, so a subrotating gradient wind balance cannot be ruled out, but it would have to be the result of dynamical mechanisms other than those we have considered.

c. *How Similar Are Venus and Titan?*

We have argued that Titan is likely to be in the same superrotating regime as Venus. The difference between Experiments T3 and V attests, however, to the presence of special conditions on Venus which allow superrotation to exist. In Gierasch's theory, U is proportional to Ωa, which is a factor of 6 smaller for Venus than for Titan. Thus, for the same depth of flow and vertical mixing, we would expect much weaker winds on Venus. However, superrotating flow is seven scale heights deep on Venus, which means that strong cloud-top winds can exist despite moderate vertical shear. By comparison, the GCM we have used is only two to three scale heights deep, which may be sufficient for Titan's troposphere but is not for Venus'. The relatively weak surface source of momentum at Venus' rotation rate suggests that simulation of that planet's dynamics is much more sensitive to energy dissipation and artificial momentum sinks in the model. Comparison of the energy cycles in Experiments T3 and V bears this out. From a modeling standpoint, either a thicker cloud than we have used or one with latitudinally varying radiative properties may be necessary, in order that radiatively driven convective layers be separated vertically and horizontally from the location of the jet. (On Venus, the neutrally stable middle cloud layer is two to three scale heights below cloud top, and cloud feature morphology changes from cellular to linear in midlatitudes.) Numerical schemes which conserve momentum to higher accuracy and conservative gravity wave drag parameterizations are also required.

Of course, astronomical factors should be considered in any comparison of Venus and Titan dynamics. Titan's greater distance from the Sun implies weaker radiative driving, but the primary effect may be to make Titan's radiative time constant comparable to that of the much thicker Venus atmosphere. Semidiurnal tides have been shown to significantly amplify superrotation near the Venus cloud top (Hou *et al.* 1990), so that the Gierasch–Rossow–Williams mechanism need not provide all of the angular momentum. Given Titan's long radiative time constants at all altitudes, tidal driving is likely to be less important there. On the other hand, Venus' small obliquity should effectively eliminate seasonal effects there, while seasonality may have important dynamical consequences on Titan (Flasar and Conrath 1990).

Finally, we note that despite the need for model improvements, our results for Titan seem to be easily understood in terms of well-resolved dynamical mechanisms and seem at least qualitatively robust to changes in uncertain parameters. Furthermore, experiments underway with other models (Hourdin *et al.* 1992) are producing results similar to ours in their spinup stage. We therefore conclude that equatorial superrotation is probably a common feature of statically stable, slowly rotating planets.

ACKNOWLEDGMENTS

Many of the ideas in this paper were formulated during stimulating discussions with M. Allison and W. Rossow. We appreciate the helpful comments of P. Gierasch, R. Young, and an anonymous reviewer. Some preliminary computations were performed by J. Thorburn during the 1987 Summer Institute on Atmospheric Sciences organized by GISS and GSFC. This work was supported by the NASA Planetary Atmospheres Program.

REFERENCES

ALLISON, M., 1992. A preliminary assessment of the Titan planetary boundary layer. In *Titan* (B. Kaldeich, Ed.), pp. 113–118. ESA SP-338, Noordwijk.

ALLISON, M., AND L. D. TRAVIS 1986. Astronomical, physical, and meteorological parameters for planetary atmospheres. In *The Jovian Atmospheres* (M. Allison and L. D. Travis, Eds.), pp. 293–319. NASA CP-2441, Washington, DC.

ALLISON, M., AND A. D. DEL GENIO 1992. A zero potential vorticity model for the zonal-mean circulation of the Venus/Titan atmospheres. *J. Atmos. Sci.*, in press.

ARAKAWA, A. 1972. Design of the UCLA general circulation model. Tech. Rep. No. 7, Dept. Meteor., University of California, Los Angeles.

COVEY, C., E. J. PITCHER, AND J. P. BROWN 1986. General circulation model simulations of superrotation in slowly rotating atmospheres: Implications for Venus. *Icarus* **66,** 380–396.

DEL GENIO, A. D., AND W. B. ROSSOW 1982. Temporal variability of ultraviolet cloud features in the Venus stratosphere. *Icarus* **51,** 391–415.

DEL GENIO, A. D., AND R. J. SUOZZO 1987. A comparative study of rapidly and slowly rotating dynamical regimes in a terrestrial general circulation model. *J. Atmos. Sci.* **44,** 973–986.

DEL GENIO, A. D., AND W. B. ROSSOW 1990. Planetary-scale waves and the cyclic nature of cloud top dynamics on Venus. *J. Atmos. Sci.* **47,** 293–318.

FELS, S. B., AND R. S. LINDZEN 1974. The interaction of thermally excited gravity waves with mean flows. *Geophys. Fluid Dyn.* **6,** 149–191.

FLASAR, F. M. 1983a. The meteorology of methane in Titan's troposphere. *Bull. Am. Astron. Soc.* **15,** 843–844.

FLASAR, F. M. 1983b. Oceans on Titan. *Science* **221,** 55–57.

FLASAR, F. M., R. E. SAMUELSON, AND B. J. CONRATH 1981. Titan's atmosphere: Temperature and dynamics. *Nature* **292,** 693–698.

FLASAR, F. M., AND B. J. CONRATH 1990. Titan's stratospheric temperatures: A case for dynamical inertia? *Icarus* **85,** 346–354.

GIERASCH, P. J. 1975. Meridional circulation and the maintenance of the Venus atmospheric rotation. *J. Atmos. Sci.* **32,** 1038–1044.

GIERASCH, P. J. 1987. Waves in the atmosphere of Venus. *Nature* **328,** 510–512.

GOLD, T., AND S. SOTER 1971. Atmospheric tides and the 4-day circulation on Venus. *Icarus* **14,** 16–20.

HANSEN, J., G. RUSSELL, D. RIND, P. STONE, A. LACIS, S. LEBEDEFF, R. RUEDY, AND L. TRAVIS 1983. Efficient three-dimensional global models for climate studies: Models I and II. *Mon. Weather Rev.* **111,** 609–662.

HELD, I. M., AND A. Y. HOU 1980. Nonlinear axially symmetric circulations in a nearly inviscid atmosphere. *J. Atmos. Sci.* **37,** 515–533.

HIDE, R. 1969. Dynamics of the atmospheres of the major planets with an appendix on the viscous boundary layer at the rigid bounding surface of an electrically-conducting rotating fluid in the presence of a magnetic field. *J. Atmos. Sci.* **26,** 841–853.

HOU, A. Y., AND B. F. FARRELL 1987. Superrotation induced by critical-level absorption of gravity waves on Venus: An assessment. *J. Atmos. Sci.* **44,** 1049–1061.

HOU, A. Y., S. B. FELS, AND R. M. GOODY 1990. Zonal superrotation above Venus' cloud base induced by the semidiurnal tide and the mean meridional circulation. *J. Atmos. Sci.* **47,** 1894–1901.

HOUGHTON, J. T. 1977. *The Physics of Atmospheres*. Cambridge Univ. Press, Cambridge.

HOURDIN, F., P. LE VAN, O. TALAGRAND, R. COURTIN, D. GAUTIER, AND C. P. MCKAY 1992. Numerical simulation of the circulation of the atmosphere of Titan. In *Titan* (B. Kaldeich, Ed.), pp. 101–106. ESA SP-338, Noordwijk.

KUO, H.-L. 1949. Dynamical instability of two-dimensional and nondivergent flow in a barotropic atmosphere. *J. Meteor.* **6,** 105–122.

KUO, H.-L. 1978. A two-layer model study of the combined barotropic and baroclinic instability in the tropics. *J. Atmos. Sci.* **35,** 1840–1860.

LEOVY, C. B. 1973. Rotation of the upper atmosphere of Venus. *J. Atmos. Sci.* **30,** 1218–1220.

LEOVY, C. B. 1987. Zonal winds near Venus' cloud top level: An analytic model of the equatorial wind. *Icarus* **69,** 193–201.

LINDAL, G. F., G. E. WOOD, H. B. HOTZ, D. N. SWEETNAM, V. R. ESHLEMAN, AND G. L. TYLER 1983. The atmosphere of Titan: An analysis of the Voyager 1 radio occultation measurements. *Icarus* **53,** 348–363.

LUNINE, J. I., D. J. STEVENSON, AND Y. YUNG 1983. Ethane ocean on Titan. *Science* **222,** 1229–1230.

MAYR, H. G., AND I. HARRIS 1983. Quasi-axisymmetric circulation and superrotation in planetary atmospheres. *Astron. Astrophys.* **121,** 124–136.

MCKAY, C. P., J. B. POLLACK, AND R. COURTIN 1989. The thermal structure of Titan's atmosphere. *Icarus* **80,** 23–53.

MUHLEMAN, D. O., A. W. GROSSMAN, B. J. BUTLER, AND M. A. SLADE 1990. Radar reflectivity of Titan. *Science* **248,** 975–980.

PECHMANN, J. B., AND A. P. INGERSOLL 1984. Thermal tides in the atmosphere of Venus: Comparison of model results with observations. *J. Atmos. Sci.* **41,** 3290–3313.

POLLACK, J. B., AND R. YOUNG 1975. Calculations of the radiative and dynamical state of the Venus atmosphere. *J. Atmos. Sci.* **32,** 1025–1037.

ROSSOW, W. B. 1983. A general circulation model of a Venus-like atmosphere. *J. Atmos. Sci.* **40,** 273–302.

ROSSOW, W. B. 1985. Atmospheric circulation of Venus. *Adv. Geophys.* **28A,** 347–379.

ROSSOW, W. B., AND G. P. WILLIAMS 1979. Large-scale motion in the Venus stratosphere. *J. Atmos. Sci.* **36,** 377–389.

ROSSOW, W. B., A. D. DEL GENIO, AND T. EICHLER 1990. Cloud-tracked winds from Pioneer Venus OCPP images. *J. Atmos. Sci.* **47,** 2053–2084.

SAMUELSON, R. E. 1983. Radiative equilibrium model of Titan's atmosphere. *Icarus* **53,** 364–387.

SICARDY, B., A. BRAHIC, C. FERRARI, D. GAUTIER, J. LECACHEUX, E. LELLOUCH, F. ROQUES, J. E. ARLOT, F. COLAS, W. THUILLOT, F. SEVRE, J. L. VIDAL, C. BLANCO, S. CRISTALDI, C. BUIL, A. KLOTZ, AND E. THOUVENOT 1990. Probing Titan's atmosphere by stellar occultation. *Nature* **343,** 350–353.

STONE, P. H. 1974. The structure and circulation of the deep Venus atmosphere. *J. Atmos. Sci.* **31,** 1681–1690.

TOMASKO, M. G., L. R. DOOSE, P. H. SMITH, AND A. P. ODELL 1980. Measurements of the flux of sunlight in the atmosphere of Venus. *J. Geophys. Res.* **85,** 8167–8186.

WENKERT, D. D., AND G. W. GARNEAU 1987. Does Titan's atmosphere have a 2-day rotation period? *Bull. Am. Astron. Soc.* **19,** 875.

WILLIAMS, G. P. 1988a. The dynamical range of global circulations—I. *Climate Dyn.* **2,** 205–260.

WILLIAMS, G. P. 1988b. The dynamical range of global circulations—II. *Climate Dyn.* **3,** 45–84.

YOUNG, R. E., AND J. B. POLLACK 1977. A three-dimensional model of dynamical processes in the Venus atmosphere. *J. Atmos. Sci.* **34,** 1315–1351.

YOUNG, R. E., R.L. WALTERSCHEID, G. SCHUBERT, A. SEIFF, V. M. LINKIN, AND A. N. LIPATOV 1987. Characteristics of gravity waves generated by surface topography on Venus: Comparison with the VEGA balloon results. *J. Atmos. Sci.* **44,** 2628–2639.